seems quite possible that the approximations made here and those inherent to the Hartree-Fock framework make the results for an atom with 18 electrons very much in error.[7]

In the alkaline-earth K values there are only three exceptions and these are not entirely unexpected. All values in this column are greater than unity or approximately unity except for the three negative ions. Also, excluding the negative ions again, they all decrease with increasing Z. It would seem most likely that the anomalous behavior of the Li^-, Na^-, and K^- functions is due to the inherent inadequacy of the Hartree-Fock description of negative ions.

ACKNOWLEDGMENT

It is a pleasure to thank Professor A. David Buckingham for several helpful discussions and suggestions during the course of this work.

PHYSICAL REVIEW VOLUME 162, NUMBER 1 5 OCTOBER 1967

Stark Broadening of H_β, H_γ, and H_δ: An Experimental Study*

R. A. Hill and J. B. Gerardo
Sandia Laboratory, Albuquerque, New Mexico
(Received 11 May 1967)

Stark-broadened H_β, H_γ, and H_δ line profiles from a spatially uniform plasma column which was formed in a critically damped discharge tube were recorded with a rapid-scan spectrometer. A plasma temperature of ~ 2 eV was inferred from both H_β- and H_γ-to-continuum ratios. Values of the electron density were determined to an estimated accuracy of better than $\pm 2\%$ by means of two multiple-pass laser interferometers operating at infrared and visible wavelengths. Systematic errors in recording and analyzing the line profiles are estimated to be less than $\pm 1.5\%$. For interferometric values of the electron density in the range $(1.3-8.5)\times 10^{16}$ cm^{-3}, the measured half-intensity widths of all the recorded H_β profiles agreed to within $\pm 2\%$ of the widths predicted by Stark-broadening theory. In this comparison, the $\pm 2\%$ represents the maximum scatter of the measured half-intensity widths where the theoretical widths were determined using the interferometric values of electron density which were taken as the standard. The total systematic error in this comparison is estimated to be less than $\pm 3.5\%$. For H_γ the measured half-intensity widths ranged from 11 to 25% larger than that predicted by theory for electron densities in the range $(1.3-7.1)\times 10^{16}$ cm^{-3}. For H_δ the measured half-intensity widths are 7% narrower than that predicted by theory for electron densities in the range $(1.3-2.8)\times 10^{16}$ cm^{-3}. Because the H_β, H_γ, and H_δ profiles were recorded from the same plasma, systematic errors in measuring the electron density will affect the comparison of theory and experiment for each line in the same sense. Thus the relative systematic errors between the comparison of all three lines with the theory are estimated to be less than $\pm 1.5\%$.

I. INTRODUCTION

THE dominant line-broadening mechanism in dense plasmas ($N_e > 10^{15}$ cm^{-3}, $T_e < 10$ eV) is Stark broadening caused by the electric microfields of the free electrons and ions which surround the radiating atoms. Because hydrogen is subject to a linear Stark effect, the Balmer lines experience a pronounced Stark broadening which depends almost entirely on the charged-particle density. Thus, experimentally obtained Stark profiles can be used as a measure of electron density provided the relationship between broadening and electron density is well known.

Previous experimental studies of Stark-broadened Balmer lines emitted by arcs[1,2] and shock tubes[3] indicated significant inadequacies in the old Holtzmark theory.[4] The development of a generalized impact approximation by Kolb and Griem[5] and independently by Baranger[6] led to an improved Stark-broadening theory which included the effects of electrons, Debye shielding, and ion-ion correlations.[7,8] Theoretical profiles have been tabulated by Griem[9] which are estimated to have an over-all accuracy of better than 15%. This corresponds to a possible error of $\pm 20\%$ in the electron densities deduced from recorded profiles.[8]

Among the several groups who performed previous experimental checks of the theory, Berg *et al.*[10] found that the Stark theory for H_α, H_β, and H_γ predicted

* This work was supported by the U. S. Atomic Energy Commission.
[1] H. Griem, Z. Physik **137**, 280 (1954).
[2] P. Bogen, Z. Physik **149**, 62 (1957).
[3] L. R. Doherty and E. B. Turner, Astron. J. **60**, 158 (1955).
[4] J. Holzmark, Ann. Physik **58**, 577 (1919); Physik Z. **20**, 162 (1919); **25**, 73 (1924).
[5] A. C. Kolb and H. R. Griem, Phys. Rev. **111**, 514 (1958).
[6] M. Baranger, Phys. Rev. **111**, 494 (1958).
[7] H. R. Griem, A. C. Kolb, and K. Y. Shen, Phys. Rev. **116**, 4 (1959).
[8] H. R. Griem, A. C. Kolb, and K. Y. Shen, Astrophys. J. **135**, 272 (1962).
[9] H. R. Griem, *Plasma Spectroscopy* (McGraw-Hill Book Company, Inc., New York, 1964).
[10] H. F. Berg, A. W. Ali, R. Lincke, and H. R. Griem, Phys. Rev. **125**, 199 (1962).

values of the electron density about 4% too small at $N_e \sim 9\times10^{16}$ cm^{-3}. Wiese *et al.*,[11] found that the Stark theory for H_β and H_γ predicted values of the electron density about 12 and 25% too large, respectively, for densities in the range $(3\text{–}8)\times10^{16}$ cm^{-3}. McLean and Ramsden[12] found that the Stark theory for H_β predicted values of the electron density to within $\pm6\%$ at 1.2×10^{17} cm^{-3}.

The results of a recent experimental investigation of Stark-broadening theory for the electron density range $(2\text{–}4)\times10^{16}$ cm^{-3} indicate that the estimated accuracy of the theoretical H_β profiles is somewhat pessimistic.[13] It is shown here that this excellent agreement between theory and experiment, $\pm3.5\%$, extends over the electron density range $(1.3\text{–}8.5)\times10^{16}$ cm^{-3}. In addition, accurate checks on the Stark theory for H_γ and H_δ are presented. The high accuracy of these measurements was obtained by using a rapid-scan spectrometer to record the Stark-broadened line profiles,[14] multiple-pass laser interferometers to independently measure the electron density,[15] and a long uniform plasma source in order to minimize boundary-layer effects. The rapid-scan spectrometer is particularly suitable for these measurements because it permits the photoelectric recording of an entire line profile in a time short compared to the decay time of the transient plasma. Laser interferometers provide a particularly suitable method for independent measurement of the electron density because improved accuracy can be easily obtained through the use of multiple-pass techniques and infrared wavelengths.

In order to justify the high accuracy claimed in this paper, particular attention is given in the following sections to (a) the effect of the wavelength dependence of the polarizabilities of the neutral and excited state atoms on the interferometric measurements, (b) the effect of the finite slit widths and finite rise-times of the recording electronics on the recorded line profiles, and (c) the effect of volume and boundary-layer absorption on the shapes of the recorded profiles.

II. INTERFEROMETRIC MEASUREMENTS OF ELECTRON DENSITY

Multiple-pass laser interferometers at both visible and infrared wavelengths were used to measure the plasma electron density. The particular geometry used here is illustrated in Fig. 1. The only significant difference between the laser interferometers used here and those previously described[15–17] is in the use of a very high reflection coefficient ($\rho>99.9\%$) for mirror M_2. This prevents the amplitude of the laser from being significantly modulated and thus eliminates the hybrid wave form[16] of the detected interferometer signal.

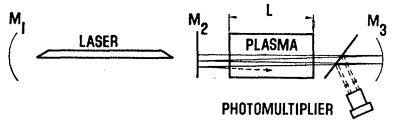

FIG. 1. Optical arrangement for a multiple-pass laser interferometer. The laser cavity is formed by mirrors M_1 and M_2; the multiple passes occur through the plasma between mirrors M_2 and M_3.

The number of cycles of modulation (fringes) observed by the photomultiplier for a given change in the index of refraction Δn of the plasma is given by

$$\chi=2S\Delta nL/\lambda, \tag{1}$$

where S is the number of discrete passes[15] made by radiation of wavelength λ through a plasma medium of length L. Equation (1) assumes that the index of refraction is uniform along the length of the traversed plasma. If this is not the case, the product ΔnL must be replaced by the line integral $\int_0^L \Delta n(l)dl$. The index of refraction is related to the electron density and the atomic and molecular constituent densities by

$$n=1-\frac{1}{2}\left(\frac{\omega_p}{\omega}\right)^2+2\pi\sum_n \alpha_n N_n, \tag{2}$$

where $\omega=2\pi c/\lambda$, $\omega_p^2=N_e e^2/\epsilon_0 m$, ϵ_0 is the permittivity of free space, e and m are the electronic charge and mass, N_n is the number density of atoms (or not completely stripped ions) in the nth quantum state, and α_n is the polarizability of this electronic state. If the index of refraction is measured at two different wavelengths and if the wavelength dependence of the constituent polarizabilities can be neglected, the electron density is given by

$$N_e=\frac{1.247\times10^{13}}{L(\lambda_1^2-\lambda_2^2)}\left(\frac{\chi_1\lambda_1}{S_1}-\frac{\chi_2\lambda_2}{S_2}\right), \tag{3}$$

where χ_1 and χ_2 represent the number of fringes observed at the laser wavelengths λ_1 and λ_2, respectively. Obviously, Eq. (3) requires that neither of the laser wavelengths coincide with a characteristic transition wavelength of the plasma because of the strong wavelength dependence of α_n near a line center. Even if the laser wavelengths are far removed from all characteristic radiation, there is a small inaccuracy introduced in the electron density measurement by neglecting the wavelength dispersion of the α_n's. This inaccuracy is strongly

[11] W. L. Wiese, D. R. Paquette, and J. E. Solarski, Phys. Rev. **129**, 1225 (1963).
[12] E. A. McLean and S. A. Ramsden, Phys. Rev. **140**, A1122 (1965).
[13] J. B. Gerardo and R. A. Hill, Phys. Rev. Letters **17**, 623 (1966).
[14] R. A. Hill and R. D. Fellerhoff, Appl. Opt. **5**, 1105 (1966).
[15] J. B. Gerardo and J. T. Verdeyen, Proc. IEEE **52**, 690 (1964).
[16] J. B. Gerardo, J. T. Verdeyen, and M. A. Gusinow, J. Appl. Phys. **36**, 2146 (1965).
[17] J. B. Gerardo, J. T. Verdeyen, and M. A. Gusinow, J. Appl. Phys. **36**, 3526 (1965).

dependent on the nature of the plasma. For the case of a high-temperature hydrogen plasma, the error in Eq. (3) can be estimated as follows. If the wavelength of the radiation is far removed from all characteristic radiation λ_{mn}, the contribution to the refractivity by neutral atoms in state n is [9]

$$2\pi\alpha_n N_n=\sum_{m>n}\frac{r_0 f_{mn}\lambda_{mn}^2}{2\pi}\left[1+\left(\frac{\lambda_{mn}}{\lambda}\right)^2+\cdots\right]N_n, \quad (4)$$

where f_{mn} is the absorption oscillator strength and $r_0=2.82\times10^{-13}$ cm is the classical electron radius. The electron temperature of the hydrogen plasma in these experiments is nominally 2 eV and, therefore, to a good approximation all excited levels are collision dominated. Consequently, the excited state population densities are given by the Saha equation which, for a hydrogen plasma, is

$$N_n=n^2N_e^2\left(\frac{h^2}{2\pi mkT}\right)^{3/2}\exp\left(\frac{E_i}{n^2kT}\right), \quad (5)$$

where E_i is the ionization energy of the ground-state hydrogen atom. This shows that for the plasma parameters considered here ($T\sim20\,000$°K and $N_e\sim10^{16}$ cm^{-3}), the inequality $N_n\ll N_e$, $n>1$ is satisfied. Consequently, at wavelengths far removed from all characteristic radiation the only significant contribution to the refractivity by neutral atoms is by atoms in the ground state. Hence, only $n=1$ need be considered in Eq. (2) and it follows that in Eq. (4) $\lambda_{m1}\leq1215$ Å (Lyman α). The refractivity contribution given by Eq. (4) is approximately 3% larger at $\lambda_2=0.6328\,\mu$ than it is at $\lambda_1=1.1523\,\mu$. However, the error introduced in Eq. (3) by neglect of this variation is much less than 3%, as can be seen by the more correct form of Eq. (3) which includes the wavelength dependence of α_n. This requires that the term

$$-\sum_m\frac{\lambda_{mi}^4 f_{mi}}{\lambda_1^2\lambda_2^2}\Delta N_1$$

be added to the right-hand side of Eq. (3). In this notation ΔN_1 represents the change in the ground-state population density. For the wavelengths considered here, the coefficient of ΔN_1 is less than 10^{-3}. If $\Delta N_1\approx N_e$ (this is a good approximation if the plasma is highly ionized), then it follows that Eq. (3) is accurate to better than 0.1%.

The above may not be true if either λ_1 or λ_2 is in close proximity to an emission line. In this case if $\lambda=\lambda_{mn}+\Delta\lambda$ is on the far wings of a line, the contribution to the refractivity is given by[9]

$$2\pi\alpha_n N_n=\frac{r_0 f_{mn}\lambda_{mn}^3}{4\pi\Delta\lambda}\left[1-\exp\left(-\frac{E_{mn}}{kT}\right)\right]N_n, \quad (6)$$

where LTE has been assumed. This equation applies only on the far wings and $\Delta\lambda\ll\lambda_{mn}$. Giving due consideration to the terms f_{mn}, λ_{mn}, E_{mn}, and N_n, it is seen that usually no more than one line will significantly contribute to the plasma refractivity at a given wavelength. For example, at wavelength $\lambda_2=6328$ Å, the most significant contributor is the line H_α at $\lambda_{32}=6562.8$ Å. The ratio of this contribution to the refractivity to that by the free electrons is

$$\frac{f_{32}\lambda_{32}^3}{2\Delta\lambda\lambda^2}\left[1-\exp\left(-\frac{E_{32}}{kT}\right)\right]\frac{N_2}{N_e}. \quad (7)$$

At an electron temperature of 2 eV and with the aid of Eq. (5), this ratio reduces to approximately $10^{-20}N_e$, where N_e is expressed in cm^{-3}. Hence, with electron densities less than 10^{17} cm^{-3}, this effect will not significantly contribute to the refractivity of the plasma. A similar argument will show that this is also true at wavelength $\lambda_1=1.1523\,\mu$.

Some uncertainty remains as to the effect on the plasma refractivity by electrons in very highly excited bound states. All electrons in states that are separated from the reduced ionization limit by less than the photon energy hc/λ are practically indistinguishable from the free electrons.[9] Hence, these electrons should be included in the term $\frac{1}{2}(\omega_p/\omega)^2=r_0\lambda^2N_e/2\pi$ and N_e in Eq. (3) is the sum of the free-electron density and those electrons in the relevant highly excited states. Typically, this correction to the electron density is less than 1%.[9] Fortunately, the highly excited bound electrons also contribute to Stark broadening[9] as if they were free electrons. The number of states involved in this contribution is not identical to the number of bound states which contribute to the refractivity but in general they do not differ significantly. It is expected that the difference is at most a few tenths of a percent.

III. RAPID-SCAN RECORDING OF LINE PROFILES

The optical arrangement of the rapid-scan spectrometer used here is illustrated in Fig. 2. For a complete description of this device the reader is referred to Ref. 14. Light from the plasma is focused on the en-

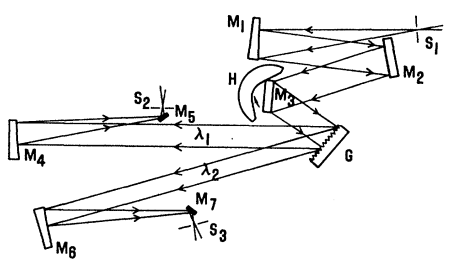

FIG. 2. Optical arrangement in the rapid-scan spectrometer. S_1, entrance slit; M_1, M_4, and M_6, off-axis paraboloidal mirrors; M_2, M_5, and M_7, flat mirrors; M_3, high-speed rotating mirror; G, plane grating (600 l/mm); S_2 and S_3, exit slits.

trance slit S_1 and is collimated by a 381-mm-focal-length off-axis paraboloidal mirror M_1. Mirror M_2 directs this light to a high-speed rotating mirror M_3. The motion of this rotating mirror causes the collimated light to be scanned across the face of a plane grating G, resulting in a changing angle of incidence. The wavelength component λ_1 (λ_2) that is parallel to the axis of the off-axis paraboloidal mirror M_4 (M_6) is reflected by the pick-off mirror M_5 (M_7) through the exit slit S_2 (S_3). Thus, a portion of the spectrum is scanned at a constant angle of diffraction by each detector system, the angle of diffraction being defined by the angle between a paraboloid axis and the grating normal. The spectral scan speed is determined by the grating equation $n\lambda=d(\sin i+\sin\theta)$ and the rotational speed R of the rotating mirror. Thus, for an angle of incidence $i=0$, in the first order ($n=1$)

$$d\lambda/dt=4\pi Rd \tag{8a}$$

and

$$\lambda=\lambda_0+4\pi Rd(t-t_0), \tag{8b}$$

where d is the grating spacing and R is expressed in rps.

Denoting a photon flux from a pure Stark-broadened profile by I_λ and the normalized profile due to other broadening mechanisms (e.g., Doppler broadening) by $f(\lambda)$, the photon flux incident on the entrance slit S_1 is given by

$$I_\lambda'=\int_{-\infty}^{\infty} I_\lambda(\lambda-x)f(x)dx. \tag{9}$$

The photon flux that passes through the exit slit is expressed by the relation

$$I''(t)=I_\lambda''[\lambda=\lambda_0+4\pi Rd(t-t_0)], \tag{10}$$

where

$$I_\lambda''=A\int_{-\infty}^{\infty} I_\lambda'(\lambda-y)f'(y)dy \tag{11a}$$

$$=A\int_{-\infty}^{\infty} I_\lambda(\lambda-x)\int_{-\infty}^{\infty} f(x-y)f'(y)dydx, \tag{11b}$$

$f'(y)$ is a normalized slit function, and A is a constant. The wave form displayed on an oscilloscope will be slightly different from $I''(t)$ because of the finite rise time of the photomultiplier and oscilloscope. If the response of this electrical system to a unit step input can be represented by $V(t)=1-e^{-t/\tau}$, then the displayed wave form is given by[18]

$$I'''(t)=\frac{B}{\tau}\int_0^t I''(t-z)e^{-z/\tau}dz, \tag{12}$$

where B is the constant of proportionality between the electrical output of the photomultiplier and the incident photon flux $I''(t)$.

The spectral scan speed of the spectrometer was measured by recording a portion of a xenon spectrum at each of the rotor speeds used. The photomultiplier output was displayed on the upper beam of a Tektronix 551 dual-beam oscilloscope and timing pulses, derived from a crystal controlled oscillator, were recorded on the lower trace for a sweep calibration of the recording scope. A least-squares fit of 20 xenon lines to the timing marks gave a spectral scan speed of 83.65 ± 0.10 Å/μsec for a rotor speed of $\sim$400 rps. The range is a simultaneous confidence interval for a confidence limit of 95%.[19] This spectral scan speed is reproducible to within $\pm0.15\%$ on a shot-to-shot basis.

The slit function was experimentally determined by recording essentially unbroadened lines from a cold xenon plasma. This was performed for each combination of spectral scan speed and slit width which was used while recording the Balmer profiles. These recorded xenon profiles represent the slit function $f'(\lambda)$modified by the electrical circuit response as given by Eq. (12). In order to determine the slit function from the recorded profiles, a set of Voigt profiles was folded with the circuit response according to Eq. (12) using the measured time constant $\tau=6\times10^{-9}$ sec. A comparison of the half-intensity and tenth-intensity widths of the recorded profiles with the respective widths of the modified Voigt profiles indicated that at each spectral scanning speed and slit width, the slit function was best represented by a Gaussian function. For example, at a rotor speed of 400 rps and entrance and exit slit widths of 15 μ each, the measured half-intensity and tenth-intensity widths are 1.75 and 3.34 Å, respectively. These measured values compare favorably with those of a Gaussian profile having a half-intensity width of 1.50 Å which after modification by the circuit time constant, gives 1.75 and 3.35 Å, respectively.

For the plasma investigated here, the only significant broadening mechanism, in addition to Stark broadening, is Doppler broadening. Thus $f(\lambda)$ is Gaussian with a half-intensity width

$$\Delta\lambda_d=\left[\frac{2kT\ln 2}{Mc^2}\right]\lambda_0.$$

Since the slit function is also Gaussian, Eq. (11b) can be written

$$I_\lambda''=A\int_{-\infty}^{\infty} I_\lambda(\lambda-x)f''(x)dx, \tag{13}$$

where $f''(x)$ is a Gaussian function of half-intensity width

$$\Delta\lambda=(\Delta\lambda_s^2+\Delta\lambda_d^2)^{1/2}$$

and $\Delta\lambda_s$ is the half-intensity width of the slit function $f'(\lambda)$.

[18] M. E. Van Valkenburg, *Network Analysis* (Prentice-Hall, Inc., Englewood Cliffs, New Jersey, 1955), p. 167.

[19] H. Scheffe, *The Analysis of Variance* (John Wiley & Sons, Inc., New York, 1959).

IV. THE PLASMA SOURCE

The plasma investigated was formed in a Pyrex wall cylinder, 3.0 cm in diameter and 14.9 cm long, which was fitted with narrow brass ring electrodes on each end. The discharge tube was filled with hydrogen gas to the desired pressure, and the plasma was produced by discharging a critically damped 2-μF capacitor between the two ring electrodes. The discharge tube was positioned in the reference cavity of the laser interferometer as is illustrated in Fig. 3. Plasma light passing through the end window from the center of the discharge tube was focused on the entrance slit of the rapid-scan spectrometer with the aid of the movable pick-off mirror. The spherical mirror located to the left of the discharge tube in Fig. 3 was used to measure self-absorption. This will be discussed in Sec. V.

The main requirement of the plasma source in this experiment is its uniformity. This was already discussed in one context in connection with Eq. (1) and the interferometric measurement of electron density. In addition, the plasma must be uniform throughout the acceptance cone of the spectrometer in order to infer a completely meaningful electron density from a single Stark-broadened profile. The plasma investigated here satisfied these requirements to the required degree. This was determined experimentally with the aid of the laser interferometers by measuring the electron density at various radii. Typical results for a gas pressure of 1.0 Torr and a capacitor voltage of 25 kV are illustrated in Fig. 4. At 0.2 cm from the side wall, the electron density fell very rapidly and this steep gradient prevented accurate density measurements in this region. The thickness of the boundary layer at the end windows of the discharge tube was assumed to be identical to that at the side walls. Hence, an effective plasma length of 14.7 cm was used in Eq. (3). The assumption of high uniformity along the length of the discharge tube was partially supported by observing the plasma "side on" with the spectrometer at various tube positions.

The maximum diameter of the spectrometer acceptance cone was 1.4 cm, which is sufficiently small so as to exclude radiation from the boundary layer of plasma at the side wall of the tube. Radiation emitted from the thin boundary layers at the two end windows

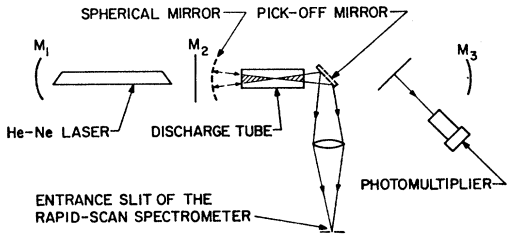

FIG. 3. A schema of the experimental setup. The pick-off mirror is moved into position only when spectra are being recorded; the spherical mirror is used to study self-absorption.

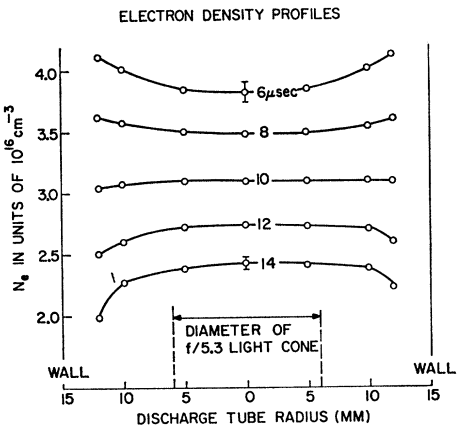

FIG. 4. Electron density profiles in the discharge tube at various times in the afterglow. The discharge was initiated at $t=0$ and the current duration was approximately 2 μsec.

was neglected since this radiation was estimated to contribute less than 1% to the total. This estimate is obtained by considering the relatively thin boundary layer at the side walls together with the N_e^2 dependence of the integrated emission coefficient in a collision-dominated plasma. The main reason for using a long plasma length is to minimize the effect of the radiation from the boundary layer. Other reasons for using a long plasma are that the error in establishing an effective plasma length for Eq. (3) will be minimized, and a larger number of fringes is obtained which increases the sensitivity of the measurement.

V. VOLUME AND WALL ABSORPTION

In order to justify the high accuracy claimed in this experiment, it is necessary to consider the extent to which the line shape is altered by self-absorption. Consider a collision-dominated plasma in which N_e, T_e, and the atom density N_a are spatially uniform. These conditions are sufficient to assure a spatially uniform emission coefficient $\epsilon(\omega)$, where $\epsilon(\omega)$ is defined as the power emitted in a specified direction in the angular frequency interval $\omega \rightarrow \omega+d\omega$ from a unit volume of plasma. The intensity of radiation emerging from the plasma is given by

$$I(\omega,L)=\frac{\epsilon(\omega)}{k'(\omega)}[1-e^{-k'(\omega)L}], \tag{14}$$

where L is the plasma length along the emission path considered and $k'(\omega)$ is the effective absorption coefficient, i.e., the difference between the true absorption and the induced emission coefficient. In the limit of small optical depth, $k'(\omega)L \ll 1$, Eq. (14) reduces to

$$I(\omega,L)=\epsilon(\omega)L[1-k'(\omega)L/2+\cdots], \tag{15}$$

which indicates that the optical depth $k'L$ must be less than 0.02 in order for the recorded profile to repre-

sent the emission profile to within an accuracy of better than 1%.

In a collision-dominated plasma, the effective absorption coefficient in a spectral line is[9]

$$k'(\omega)=2\pi^2 r_0 c f_{mn} N_n\left[1-\exp\left(-\frac{\hbar\omega}{kT}\right)\right]L(\omega), \quad (16)$$

where the levels m and n are assumed to be related by the appropriate Boltzman factor, N_n is the population density of the lower level, and $L(\omega)$ is the normalized emission line shape. Using Eq. (5) and the transformation

$$L(\omega)=\lambda^2 S(\alpha)/2\pi c F_0,$$

where $S(\alpha)$ represents the normalized line shape for the reduced wavelengths $\alpha=(\lambda_0-\lambda)/F_0$ and $F_0=2.61eN_e^{2/3}$ is the normal field strength, Eq. (16) reduces to the convenient form

$$k'=2.36n^2 N_e^{4/3}(kT)^{-3/2}\exp\left(\frac{E_i}{n^2kT}\right)f_{mn}\times\left[1-\exp\left(-\frac{\hbar\omega}{kT}\right)\right]\lambda^2 S(\alpha)\times 10^{-33}, \quad (17)$$

where k' is expressed in cm^{-1}, N_e in cm^{-3}, kT in eV, and λ in Å. Using the $S(\alpha)$ values tabulated by Griem,[9] it can be shown that in order to satisfy the inequality $I(\omega,L)/\epsilon(\omega)L\geq 0.99$ for a plasma of length $L=15$ cm and $kT=2$ eV, the electron density must be less than 2.7×10^{15}, 3.7×10^{16}, and 1.0×10^{17} for H_α, H_β, and H_γ, respectively.

The absorption was measured experimentally with the aid of the spherical mirror shown to the left of the discharge tube in Fig. 3. The center of curvature of this spherical mirror is positioned to coincide with the focal point of the optical system which focuses the plasma light on the entrance slit of the spectrometer. Thus for a collision-dominated plasma in which N_e and T_e are spatially uniform, the intensity of radiation at the right-hand boundary with the mirror in position is

$$I_m(\omega,L)=I(\omega,L)+R_c I(\omega,L)e^{-k'(\omega)L}, \quad (18)$$

where R_c is the reflection coefficient of the spherical mirror and includes any reflection or scattering losses at the windows. $I(\omega,L)$ is the intensity at the right-hand boundary of the plasma when the mirror is not in place and is related to the emission coefficient by Eq. (14). The optical depth is then determined from the measured parameters with the aid of Eq. (18):

$$k'(\omega)L=\ln\frac{R_c I(\omega,L)}{I_m(\omega,L)-I(\omega,L)}, \quad (19)$$

and thus the "true" profile can be reconstructed with the aid of Eq. (14) by substitution of the measured optical depth

$$\epsilon(\omega)L=I(\omega,L)\frac{k'(\omega)L}{1-e^{-k'(\omega)L}}, \quad (20a)$$

or in the event that $k'(\omega)L\ll 1$,

$$\epsilon(\omega)L=\frac{2R_c I^2(\omega,L)}{I_m(\omega,L)+I(\omega,L)(R_c-1)}. \quad (20b)$$

The reflection coefficient R_c is experimentally determined from measurements, with and without the spherical mirror, of the line wings which are negligibly absorbed. The reconstruction of the line profiles by Eqs. (19), (20a), and (20b) does not account for absorption by the cold boundary layer at the tube windows which can be especially important for those lines with an unshifted central Stark component, e.g., H_α and H_γ. However, it can be shown that if the two boundary layers are identical and the radiation from the boundary layers is negligible and if $k'K\ll 1$, then Eq. (19) is still applicable.

VI. EXPERIMENTAL RESULTS

Stark-broadening theory was investigated over the electron density range $(1.3\text{–}8.5)\times10^{16}$ cm^{-3} by using the three different sets of initial conditions which are listed in Table I. The uniformity of the plasmas generated at the lower and higher pressure is comparable to that mentioned earlier for the 1.0-Torr plasma. A typical laser interferogram, recorded from the 1.0-Torr plasma, is shown in Fig. 5(a). The discharge is initiated at the instant of time corresponding to laser signal maximum (signal increases downward) by means of the internal trigger on the Tektronix 551 oscilloscope. The accuracy with which the fringe shifts can be measured is estimated to be $\pm1/15$ of a fringe. Since $\lambda_1/S_1\gg\lambda_2/S_2$, the accuracy of the measured quantity in Eq. (3), $(\chi_1\lambda_1/S_1-\chi_2\lambda_2/S_2)$, is determined predominantly by the accuracy of the fringe shift measurement χ_1. Thus with a nominal fringe shift of the five full fringes, the accuracy with which this quantity is measured is $\pm1.3\%$.

The reproducibility of the plasma on consecutive discharges was determined by the laser data. Approximately seven out of eight consecutive discharges reproduced the fringe pattern of the 1.1523-μ laser interferometer to within the accuracy with which the fringes could be measured. This excellent reproducibility allowed the

TABLE I. Experimental conditions.

$N_e(10^{16}$ cm$^{-3})$	P (Torr)	V (kV)	L (cm)	S(Å/μsec)[a]	T_e (°K)
1.3–1.8	0.75	20	15	41.83	21 000
2.4–4.0	1.0	25	15	41.83 83.65	23 000
5.0–8.5	2.5	30	11	104.6 125.5	26 000

[a] Spectral-scan speed.

laser interferograms and the appropriate line profiles to be recorded (with or without the spherical mirror) on alternate discharges.

In order to obtain good statistics on the discharge reproducibility, an experimental run usually consisted of ten consecutive discharges in which four laser interferograms, three line profiles with the mirror, and three line profiles without the mirror, were recorded alternately. An average value for the electron density was calculated for each run from an average of the fringe shift measurements. This procedure tends to reduce the inaccuracies in measuring the individual fringe patterns. Systematic errors associated with Eq. (3), e.g., errors in the effective plasma length L, neglect of the wavelength dependence of the polarizability of the excited state atoms, or any slight nonuniformity, should not account for more than an additional $\pm 1.5\%$ error in the electron density measurements. These systematic errors are not an important factor in the determination of the plasma reproducibility.

The spectral scan speeds which were used in the various density ranges are listed in Table I. An example of a typical H_β profile, obtained at a spectral scan speed of 41.83 Å/μsec and recorded with a Tektronix-type 551 oscilloscope at a sweep rate of 0.2 μsec/div (a dispersion of 8.37 Å/div) is shown in Fig. 5(b). The 5-Mc/sec pulses on the lower trace were used for an oscilloscope sweep speed calibration. The large pulse on the lower trace was obtained from a delay generator which was triggered by the discharge current. This pulse is also recorded on the lower trace of the laser interferograms and is used to time correlate the recorded profile with the fringe pattern. Because of a slight vertical nonlinearity in the type-551 oscilloscope, a type-541 oscilloscope, having excellent linearity, was used to obtain the recordings which were analyzed in detail. A third oscilloscope, operating at a slower sweep rate, was used to record the relative continuum intensity at an increased sensitivity. Representative electron temperatures, as determined by the H_β-to-continuum ratio,[9] are also listed in Table I. These values agree to within $\pm 5\%$ of the values obtained by the H_γ-to-continuum ratio. The analysis of the recorded profiles for the first four members of the Balmer series will be discussed in the following sections.

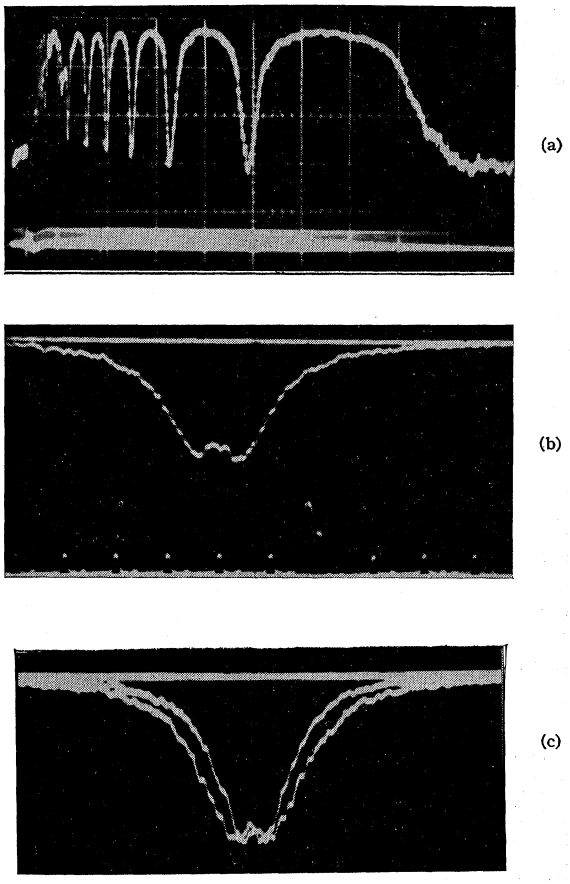

FIG. 5. Typical interferometer and spectrometer recordings. (a) The fringe pattern for $\lambda = 1.1523\ \mu$ recorded at 10 μsec/div from the 1-Torr plasma. Records obtained at a sweep rate of 2 μsec/div were used for the analysis. (b) An H_β line profile obtained at a spectral scan speed of 41.83 Å/μsec and recorded at a sweep rate of 0.2 μsec/div. The timing marks are from a 5-Mc/sec crystal-controlled oscillator. The timing pulse recorded on the lower traces of (a) and (b), is derived from the firing of the discharge tube. (c) Two superimposed H_α line profiles which were recorded with and without the spherical mirror. The peak-intensities are nearly identical showing the large self-absorption in H_α.

H_α Results

Two H_α profiles, recorded with and without the spherical mirror at an electron density of 2.74×10^{16} are shown in Fig. 5(c). The two profiles have been superimposed to better illustrate the effects of self-absorption. Because the profile with the mirror is only slightly more intense at the line center than the profile without the mirror, it is obvious that H_α is strongly self-absorbed. The central dip in these profiles is not due to the absence of a central, unshifted Stark component, but is due to a line reversal, i.e., the excitation temperature for the $n=2$ and $n=3$ states is higher at the tube center than near the walls. This is partly due to the fact that a dense layer of cold neutral particles is built up at the end windows by equilibration of pressure. In addition, in a plasma in which the excited state population densities are not totally collision dominated, the strong absorption will alter the excitation temperature of the appropriate energy levels. Since the radiation intensity is spatially dependent in an optically thick plasma—being greatest in the central regions, as can be seen with the aid of Eq. (14)—the excitation temperature will also be greater in the center of the plasma. Both of these effects can cause line reversal and thus account for the dip in the center of the recorded H_α profiles. Because of this, reconstruction of H_α profiles by means of Eq. (19) is not meaningful. Thus the

plasma source used here is not suitable for use in attempting a check on the Stark-broadening theory of H_α.

H_β Results

Stark-broadened H_β line profiles recorded with and without the spherical mirror for densities in the range $(1.3\text{–}4.0)\times10^{16}$ cm^{-3} exhibited no measurable self-absorption. Those profiles recorded in the range $(5.0\text{–}8.5)\times10^{16}$ cm^{-3} exhibited a small percentage of absorption and were thus corrected for self-absorption according to Eq. (20b). In all cases, the measured self-absorption agreed very well with the theoretical value given by Eq. (17).

A comparison of recorded and theoretical line profiles cannot be carried out directly because of the effects of the instrument functions mentioned earlier. Thus, either the recorded profiles must be compared with theoretical profiles which have been modified by the instrument functions or the theoretical profiles must be compared with experimental profiles which have been corrected for the instrument functions. To demonstrate the first technique, a theoretical profile corresponding to $N_e=2.78\times10^{16}$ cm^{-3} [the interferometric value corresponding to the recorded profile shown in Fig. 5(b)] was computed by interpolating the tables of Griem.[9] This theoretical profile was folded with the Gaussian slit function of the appropriate width (1.4 Å which includes Doppler broadening as discussed in Sec. III) by numerical integration according to Eq. (13). The resulting profile was further modified to account for the finite rise time of the recording electronics ($\tau=6\times10^{-9}$ sec, spectral scan speed$=41.83$ Å/μsec) by numerical integration according to Eq. (12). A comparison of this theoretical profile and resultant modified theoretical profile is shown in Fig. 6(a). The half-intensity width of the modified profile is 1.3% larger than that of the unmodified profile. A comparison of the recorded profile (represented by a solid line) with the modified theoretical profile (represented by points) is shown in Fig. 6(b). The agreement is excellent except near the line center where the observed dip is not as deep as the theory would indicate. The blue peak is also somewhat more intense than the red peak; however, this result is not unexpected.[9]

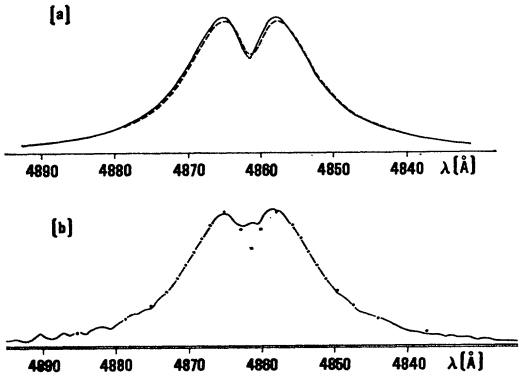

FIG. 6. (a) A theoretical profile (solid line) for $N_e=2.78\times10^{16}$ cm^{-3} [the interferometric value for Fig. 5(b)] is compared with the profile which is obtained by folding the theoretical profile with the slit and time response functions (dashed line). (b) A comparison of the experimental profile (solid line) with the modified theoretical profile (points) of (a). The narrow band at the bottom represents the continuum intensity.

The second method for comparing the recorded and theoretical profiles, as mentioned above, involves "unfolding" the instrument functions from the recorded profiles. However, instead of performing this complete "unfolding" operation, an approximate but much simpler correction technique, which requires only that the *shapes* of the theoretical and experimental profiles be similar, was employed. A set of theoretical profiles of varying half-intensity width was folded with the instrument functions according to Eqs. (12) and (13). Graphs of the increase in the $n/4$-intensity widths, $\delta\lambda_n$ ($n=1$, 2, and 3), as a function of the $n/4$-intensity widths of the modified theoretical profiles were constructed. The $n/4$-intensity widths of the recorded H_β profiles were measured after subtracting out the continuum intensity (which was measured on a separate oscilloscope) and averaging the intensities of the two peaks. These measured fractional-intensity widths were then corrected for the instrument functions by subtracting the appropriate value of $\delta\lambda$. Because the shapes of the modified theoretical profiles and the recorded profiles are very similar, this correction should be accurate to a few percent. A comparison of the corrected

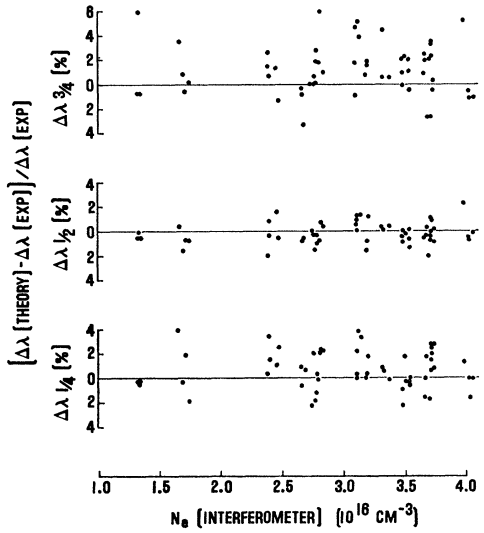

FIG. 7. A comparison of the experimental and theoretical $n/4$ intensity widths of H_β ($n=1$, 2, and 3) as a function of electron density. Two-thirds of the experimental half-intensity widths (one standard deviation) agree to within $\pm1\%$ of the theoretical half-intensity widths.

experimental and theoretical fractional-intensity widths as a function of electron density is shown in Fig. 7. The agreement between the experimental and theoretical half-intensity widths is excellent; two-thirds of the points (one standard deviation) agree to within $\pm 1.0\%$. The recorded 0.75-intensity widths are on the average approximately 1% narrower than predicted by the theory; however, the spread in the points is larger because the profiles are considerably narrower at this intensity. A comparison of the interferometric value of electron density and the value as determined by the half-intensity widths using the available tables[20] is shown in Fig. 8. These data indicate that the values of N_e as determined by Stark-broadening theory consistently agree to within $\pm 1.5\%$ of the interferometric values. Those few data points in excess of this value are attributed to the occasional slight nonreproducibility of the plasma. The estimated accuracy of the electron density measurements ($\pm 2\%$) together with the estimated systematic errors in recording and analyzing the

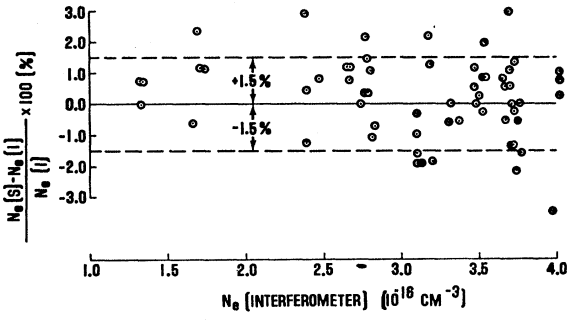

FIG. 8. A comparison of the interferometric values of electron density $N_e(I)$ with the values predicted by the half-intensity widths of the Stark-broadened H_β profiles, $N_e(S)$. Two-thirds of the points (one standard deviation) agree to within $\pm 1.5\%$.

H_β line profiles ($\pm 1.5\%$) indicate that the Stark theory for H_β is accurate to better than $\pm 3.5\%$ throughout the electron density range $(1.3\text{–}8.5)\times 10^{16}$ cm^{-3}.

H_γ Results

Two H_γ profiles, which were recorded for $N_e = 1.30 \times 10^{16}$ and 3.71×10^{16} are shown in Figs. 9(a) and 9(b), respectively. The signal-to-noise ratio for the recorded H_γ line profiles was less than in the case of H_β because of the smaller line-to-continuum ratio. These data were analyzed by averaging several profiles which were recorded on consecutive discharges in order to smooth out the noise contribution. As expected from Sec. V, the H_γ profiles recorded with and without the spherical mirror exhibited no measurable self-absorption over the density range $(1.3\text{–}7.0)\times 10^{16}$ cm^{-3}.

A comparison of the two recorded profiles shown in

[20] R. A. Hill, J. Quant. Spectry. Radiative Transfer 4, 857 (1964).

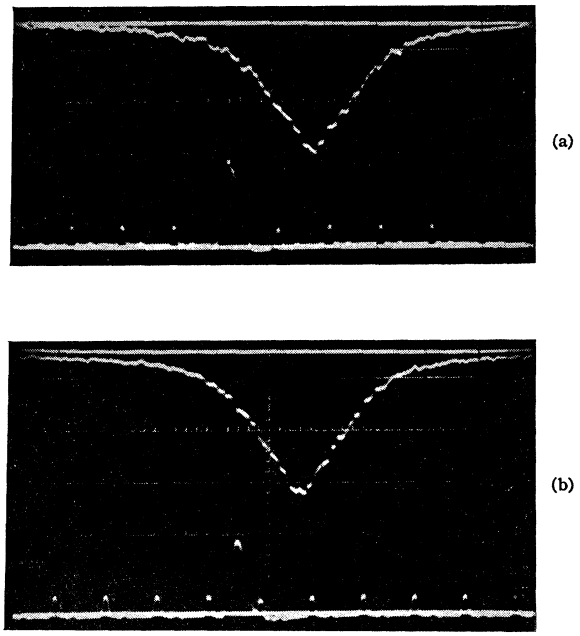

FIG. 9(a). An H_γ line profile obtained at a spectral scan speed of 41.64 Å/μsec and recorded at a sweep rate of 0.2 μsec/div for $N_e(I) = 1.30 \times 10^{16}$ cm^{-3}. (b) An H_γ line profile obtained at a spectral scan speed of 83.28 Å/μsec and recorded at a sweep rate of 0.2 μsec/div for $N_e(I) = 3.71 \times 10^{16}$ cm^{-3}.

Fig. 9 (which are represented by the solid line) and the theoretical profiles for the respective interferometric densities, including the effects of the instrument function as discussed previously, are shown in Fig. 10. The half-intensity widths of the recorded profiles are (a) 15.7 Å and (b) 32.3 Å; the half-intensity widths of the modified theoretical profiles for the respective values of electron density are: (a) 14.0 Å and (b) 27.0 Å, or a difference of 10.8 and 16.4%, respectively. Both recorded profiles exhibit slight shoulders and as in the

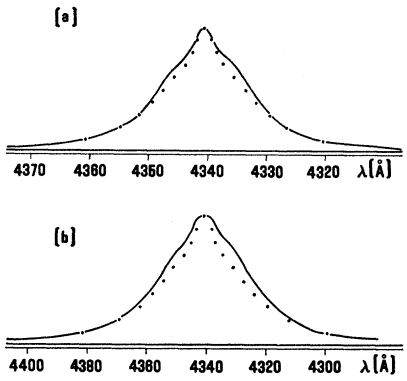

FIG. 10. Comparisons of the recorded H_γ profiles of Figs. 9(a) and 9(b) (solid lines) with the theoretical profiles for the respective densities which have been modified for the slit functions (points). The narrow band at the bottom of each profile represents the continuum intensity.

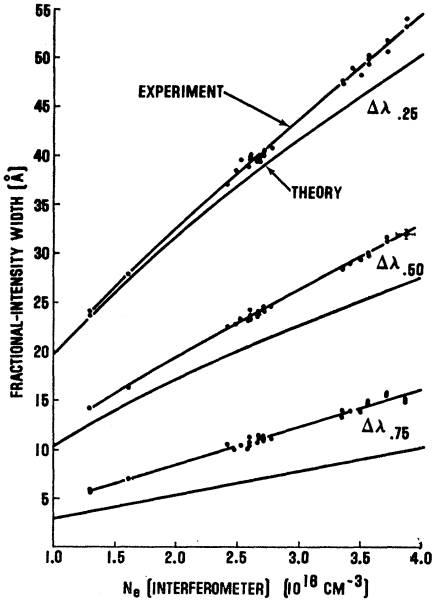

FIG. 11. A comparison of the experimental $n/4$ intensity widths (which have been corrected for the slit functions) with the theoretical $n/4$ intensity widths as a function of electron density.

example of H_β, the blue shoulder is slightly more intense than the red shoulder.

Because the general shape of the recorded and theoretical profiles is the same, the broadening effect of the instrument functions was deduced from the theoretical profiles as in the example of H_β. The measured 0.25-, 0.50-, and 0.75-intensity widths were corrected for the instrument functions and are compared with the corresponding theoretical fractional-intensity widths in Fig. 11. Because of the larger deviation between theory and experiment, the actual widths are compared instead of a percent difference as in the example of H_β. This comparison indicates that the experimental H_γ line profiles are somewhat broader than predicted by Griem.[9]

H_δ Results

The theoretical profiles for H_δ have been tabulated only for densities in the range 10^{14}–10^{16} cm^{-3} and thus an extrapolation is necessary to reach densities corresponding to the recorded profiles, $(1.3\text{–}2.8)\times10^{16}$ cm^{-3}.

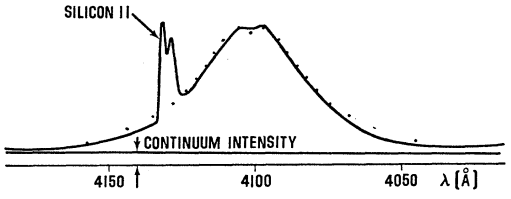

FIG. 12. A comparison of a recorded H_δ profile (solid line) with an extrapolated theoretical profile which has been modified for the slit functions. $N_e(I)=2.72\times10^{16}$ cm^{-3}. The narrow band at the bottom represents the calculated continuum intensity for a plasma temperature of 21 000°K.

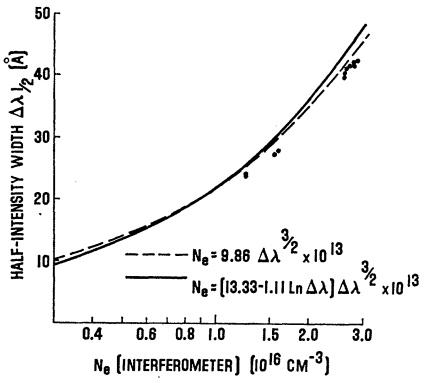

FIG. 13. A comparison of the experimental half-intensity widths (which have been corrected for the slit functions) with the theoretical half-intensity widths as a function of electron density.

The usual method of extrapolation is to assume that the half-intensity width varies as $N_e^{2/3}$, or

$$N_e=C\Delta\lambda^{3/2}\times10^{13}. \tag{21}$$

For $N_e=10^{16}$ cm^{-3} and $T_e=2\times10^4$ °K, the tabulated value[20] of $\Delta\lambda$ for H_δ is 21.74 Å and thus $C=9.86$. However, this value of C is valid only for densities close to 10^{16} cm^{-3}. For example, at $\Delta\lambda=13.20$ Å, the tabulated value of N_e is 5.01×10^{15} cm^{-3}, while the value from Eq. (21) is 4.73×10^{15}, a difference of 5.6%. A somewhat better approximation to the relationship between electron density and half-intensity width is given by the empirical expression

$$N_e=(C_0+C_1\ln\Delta\lambda)\Delta\lambda^{3/2}\times10^{13}, \tag{22}$$

where for H_δ the coefficients have the value $C_0=13.33$ and $C_1=1.11$.[21] The maximum deviation between the tabulated values of N_e and those predicted by Eq. (22) is ±0.5%. Expressions similar to Eq. (22) have been derived from the theoretical H_δ profiles for the $n/10$-intensity widths where $n=1, 2, \cdots, 10$.

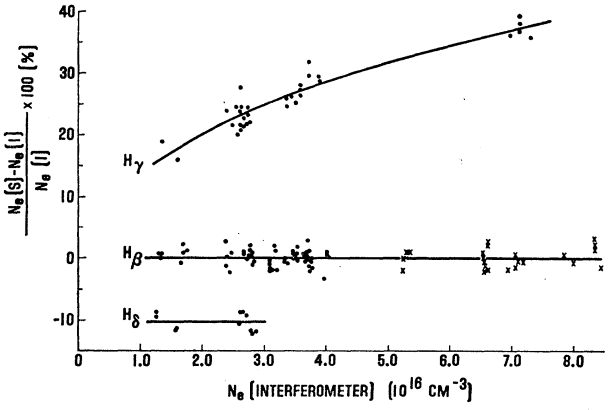

FIG. 14. A comparison of the interferometric values of electron density $N_e(I)$ with the values predicted by the half-intensity widths of the Stark-broadened H_β, H_γ, and H_δ profiles.

[21] R. A. Hill, J. Quant. Spectry. Radiative Transfer 7, 401 (1967).

TABLE II. Comparison of the theoretical and experimental Stark-broadening coefficients.

Line	Theoretical Range	C_0	C_1	Experimental Range	C_0	C_1	σ(%)
H_β	$(1\text{–}10)\times10^{16}$	35.3	−1.41	$(1.3\text{–}8.5)\times10^{16}$	34.7±1.3	−1.28±0.41	1.54
H_γ	$(1\text{–}10)\times10^{16}$	33.7	−1.72	$(1.3\text{–}7.1)\times10^{16}$	34.5±1.6	−3.78±0.47	1.36
H_δ	$(1\text{–}100)\times10^{14}$	13.3	−1.10	$(1.3\text{–}2.8)\times10^{16}$	14.6±2.0	−1.17±0.56	1.29

A comparison of an experimental H_δ profile, averaged from three consecutive discharges, and an extrapolated theoretical profile for $N_e(I)=2.72\times10^{16}$ cm^{-3} is shown in Fig. 12. The half-intensity width of the recorded profile, 42.4 Å, is 6.1% narrower than the extrapolated theoretical profile. As in the example of H_β, the blue peak is slightly more intense than the red peak, and the recorded dip is not as deep as predicted by the theory.

Because the general shape of the theoretical H_β and H_δ profiles is similar, the broadening effect of the instrument functions should be similar at a given half-intensity width. The measured half-intensity widths of the H_δ profiles were thus corrected with the instrument functions which were calculated for H_β. A comparison of these experimental values with the extrapolated theoretical half-intensity widths is shown in Fig. 13. This comparison indicates that the experimental half-intensity widths are approximately 7% narrower than predicted by the extrapolated theory.

VII. DISCUSSION

A comparison of the interferometric values of electron density and the values as determined by the half-intensity widths of H_β, H_γ, and H_δ using the available tables[20] is shown in Fig. 14. An x has been used to represent those points for H_β which required a correction for self-absorption. Two-thirds of the densities determined by the Stark-broadening theory of H_β (one standard deviation) agree to within ±1.5% of the interferometric values over the density range $(1.3\text{–}8.5)\times10^{16}$ cm^{-3}. The results for H_γ indicate that Stark-broadening theory predicts values of electron density ranging from about (16±2)% to (37±2)% too large over the density range $(1.3\text{–}7.1)\times10^{16}$ cm^{-3}. The results for H_δ indicate that the extrapolated theory predicts values of electron density about (10±2)% too small over the density range $(1.3\text{–}2.8)\times10^{16}$ cm^{-3}.

Experimental values for the coefficients C_0 and C_1 in the empirical expression relating electron density and half-intensity width [Eq. (22)] were determined by a least-squares analysis of the experimental data. Values for these coefficients and the corresponding theoretical values are listed in Table II along with the standard deviation in the points σ. The indicated ranges of the coefficients are simultaneous confidence intervals for a confidence limit of 95%.[19] The values of the coefficients for H_β and H_δ as determined from Stark-broadening theory[21] lie inside the limits given by the confidence intervals. Although the theoretical data for H_γ fit Eq. (22) only poorly, the experimental data fit this equation very well.

VIII. CONCLUSION

The results presented here are believed to represent the most precise test of the theory of Stark-broadening of H_β, H_γ, and H_δ that has been carried out to date in the electron density range $(1.3\text{–}8.5)\times10^{16}$ cm^{-3}. The high accuracy was obtained by using a uniform, reproducible plasma source having small cold boundaries, by measuring the electron density to an estimated accuracy of better than ±2.0% with multiple-pass laser interferometers, and by recording the line profiles with a rapid-scan spectrometer. Systematic errors in recording and analyzing the line profiles are estimated to be less than ±1.5%. For interferometric values of the electron density in the range $(1.3\text{–}8.5)\times10^{16}$, the measured half-intensity widths of all the recorded H_β profiles agreed to within ±2% of the widths predicted by Stark-broadening theory. In this comparison, the ±2% represents the maximum scatter of the measured half-intensity widths where the theoretical widths were determined using the interferometric values of electron density which were taken as the standard. The total systematic error in this comparison is estimated to be less than ±3.5%. Thus, the previous estimate of the accuracy of the theoretical H_β profiles, ±15%,[8] seems to be somewhat pessimistic. This may be due in part to compensating errors in the theory. For H_γ, however, the measured half-intensity widths ranged from (11±2)% to (25±2)% larger than that predicted by theory for electron densities in the range $(1.3\text{–}7.1)\times10^{16}$ cm^{-3}. This discrepancy which is comparable to that found in a previous experiment,[11] indicates that some refinement in the theoretical H_γ profiles seems to be necessary. For H_δ the measured half-intensity widths are (7±2)% narrower than those predicted by theory for electron densities in the range $(1.3\text{–}2.8)\times10^{16}$ cm^{-3}. As in the case of H_β, this discrepancy is less than the estimated accuracy of the theoretical profiles. Because the H_β, H_γ, and H_δ profiles were recorded from the same plasma, systematic errors in measuring the electron density will affect the comparison of theory and experiment for each line in the same sense. Thus the relative systematic errors between the comparisons of all three lines with the theory are estimated to be less than ±1.5%.

ACKNOWLEDGMENT

The authors are indebted to O. E. Smith for his assistance with the experiments.

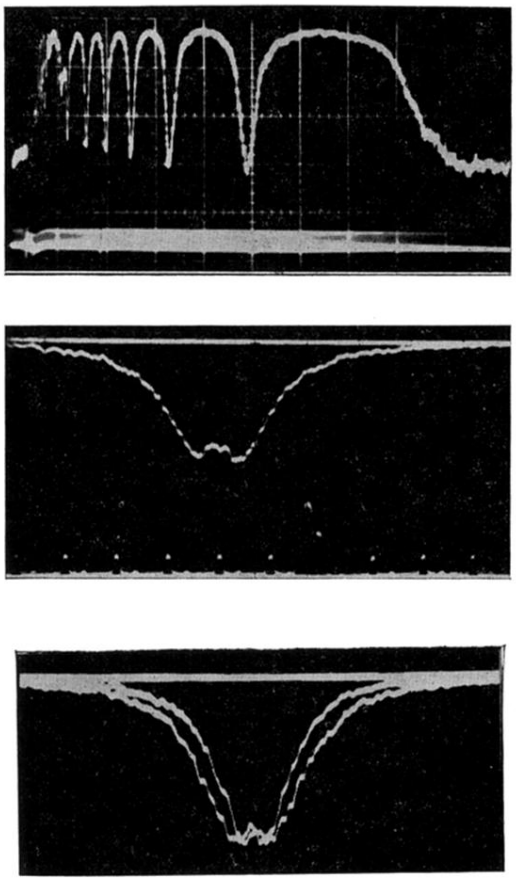

FIG. 5. Typical interferometer and spectrometer recordings. (a) The fringe pattern for $\lambda = 1.1523\,\mu$ recorded at 10 μsec/div from the 1-Torr plasma. Records obtained at a sweep rate of 2 μsec/div were used for the analysis. (b) An H_β line profile obtained at a spectral scan speed of 41.83 Å/μsec and recorded at a sweep rate of 0.2 μsec/div. The timing marks are from a 5-Mc/sec crystal-controlled oscillator. The timing pulse recorded on the lower traces of (a) and (b), is derived from the firing of the discharge tube. (c) Two superimposed H_α line profiles which were recorded with and without the spherical mirror. The peak-intensities are nearly identical showing the large self-absorption in H_α.

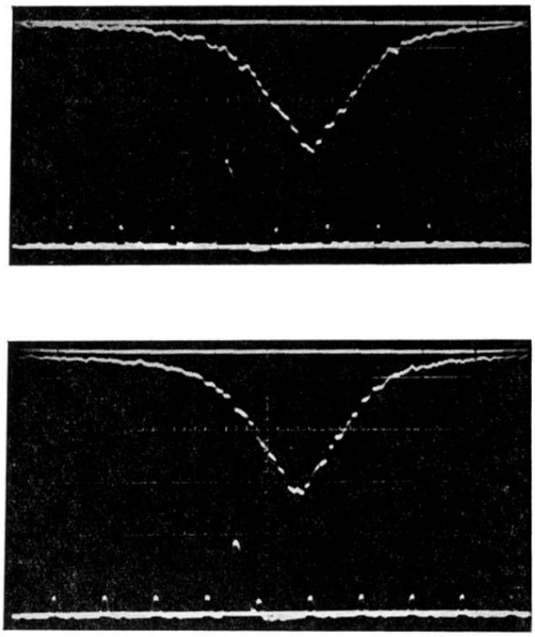

FIG. 9(a). An H_γ line profile obtained at a spectral scan speed of 41.64 Å/μsec and recorded at a sweep rate of 0.2 μsec/div for $N_e(I)=1.30\times10^{16}$ cm^{-3}. (b) An H_γ line profile obtained at a spectral scan speed of 83.28 Å/μsec and recorded at a sweep rate of 0.2 μsec/div for $N_e(I)=3.71\times10^{16}$ cm^{-3}.